JACS
JOURNAL OF THE AMERICAN CHEMICAL SOCIETY
Article
pubs.acs.org/JACS

Two-Dimensional Nanocrystals of Molecular Janus Particles

Hao Liu,[†] Chih-Hao Hsu,[†] Zhiwei Lin,[†] Wenpeng Shan,[†] Jing Wang,[†] Jing Jiang,[†] Mingjun Huang,[†] Bernard Lotz,[‡] Xinfei Yu,[†] Wen-Bin Zhang,*[,§] Kan Yue,*[,†] and Stephen Z. D. Cheng*[,†]

[†]Department of Polymer Science, College of Polymer Science and Polymer Engineering, The University of Akron, Akron, Ohio 44325-3909, United States

[‡]Institut Charles Sadron, CNRS−Université de Strasbourg, 23, Rue du Lœss, 67034 Strasbourg, France

[§]Key Laboratory of Polymer Chemistry & Physics of Ministry of Education, Center for Soft Matter Science and Engineering, College of Chemistry and Molecular Engineering, Peking University, Beijing 100871, China

Supporting Information

ABSTRACT: This paper describes a rational strategy to obtain self-assembled two-dimensional (2D) nanocrystals with definite and uniform thickness from a series of molecular Janus particles based on molecular nanoparticles (MNPs). MNPs are 3D framework with rigid shapes. Three different types of MNPs based on derivatives of polyhedral oligomeric silsesquioxane (POSS), [60]fullerene (C_{60}), and Lindqvist-type polyoxometalate (POM) are used as building blocks to construct these amphiphilic molecular Janus particles by covalently connecting hydrophobic crystalline BPOSS with a charged hydrophilic MNP. The formation of 2D nanocrystals with an exact thickness of double layers of molecules is driven by directional crystallization of the BPOSS MNP and controlled by various factors such as solvent polarity, number of counterions, and sizes of the MNPs. Strong solvating interactions of the ionic MNPs in polar solvents (e.g., acetonitrile and dimethylformamide) are crucial to provide repulsive interactions between the charged outlying ionic MNPs and suppress further aggregation along the layer normal direction. The number of counterions per molecule plays a major role in determining the self-assembled morphologies. Size matching of the hydrophobic and ionic MNPs is another critical factor in the formation of 2D nanocrystals. Self-assembly of rationally designed molecular Janus particles provides a unique "bottom-up" strategy to engineer 2D nanostructures.

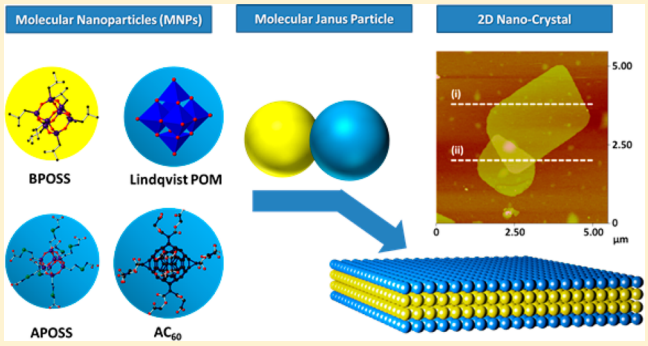

INTRODUCTION

In supramolecular chemistry,[1] the ability to control the spatial arrangement of molecules via subtle balance of various secondary interactions is the key to achieve various ordered nanostructures with different scales of hierarchy, which could possess functions that do not belong to any compositional subunits.[2] As a result, self-assembly of molecules[3] has been widely recognized as a "bottom-up" approach to engineer advanced functional nanomaterials.[4−6] Very recently, there are rapidly increasing interests in low-dimensional functional materials.[7−10] Reducing the dimensionality of bulk materials promotes the development of novel materials in many fields of nanotechnology.[11,12] Two-dimensional (2D) crystalline materials exhibit unique dimension-dependent mechanical,[13−16] electric[17−19] and optical properties,[20−23] demonstrating wide-ranging potential applications in surface property control,[24] structurally reinforced composites,[25,26] electronics,[11,27] and energy storage.[28]

2D materials with high specific surface areas have been so far generated mainly via three routes: (i) mechanical or chemical exfoliation of layered materials such as clays, graphite, boron nitrides, and many other transition metal compounds;[11,12,23] (ii) direct or templated chemical synthesis on a substrate or within a preformed framework;[21,29−33] and (iii) chemical vapor deposition.[27] Exfoliation typically involves the intercalation and delamination of corresponding bulk crystals, generally resulting in single- and multilayered nanosheets with irregular geometry and nonuniform lateral dimensions.[18] Template-assisted strategy can produce 2D nanosheets in solution, where surface stabilizing ligands are utilized to prevent vertical growth along the stacking direction of the crystals and allow only the lateral growth.[21] This method involves the chemical reaction within the template and only applies to inorganic compounds. Molecular self-assembly is an alternative approach to produce low-dimensional materials with micro- to nanometer sizes.[4−6,34] A vast majority of the intensively investigated self-assembled nanostructures are, however, 1D or 0D, such as nanofibers,[4] nanotubes,[5] and nanoparticles.[6] To date, only a few self-assembled 2D nanosheets have been reported, leaving more strategies and protocols to be demonstrated.[35−37]

Received: May 6, 2014
Published: July 9, 2014

dx.doi.org/10.1021/ja504497h | J. Am. Chem. Soc. 2014, 136, 10691−10699

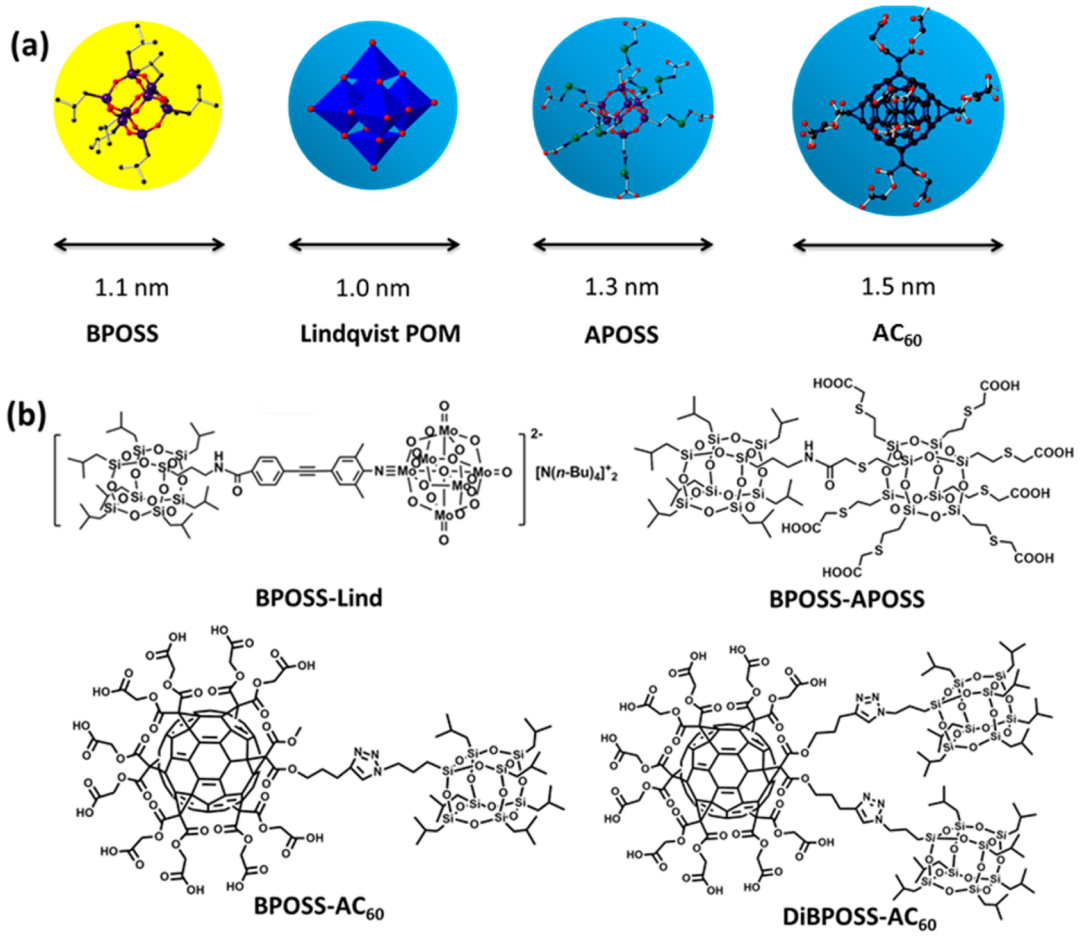

Figure 1. (a) Structures and estimated sizes of four MNPs used in this study. Yellow-colored sphere represents hydrophobic MNP, while blue-colored spheres represent hydrophilic ionic MNPs. The denoted diameters were estimated by Accelrys Cerius[2] software. (b) Chemical structures of molecular Janus particles: **BPOSS-Lind**, **BPOSS-APOSS**, **BPOSS-AC$_{60}$** and **DiBPOSS-AC$_{60}$**.

Here, we report a rationally designed strategy to generate self-assembled 2D nanocrystals from a series of molecular Janus particles without the use of a template or an exfoliation protocol. Janus particles refer to nanoparticles composed of distinct parts in composition and/or surface function.[38−41] Various methods have been developed for their preparation. Rich self-assembly behaviors of Janus particles have also been demonstrated and shown to depend on both of the intrinsic properties and external stimuli.[42−49] Molecular Janus particles are essentially nanosized amphiphilic molecules with a rigid three-dimensional (3D) conformation, which can be constructed by covalently connecting precise building blocks together. Among these promising building blocks are molecular nanoparticles (MNPs) that refer to shape- and volume-persistent molecules with 3D frameworks, including the derivatives of polyhedral oligomeric silsesquioxane (POSS),[50,51] [60]fullerene (C_{60}),[52,53] and polyoxometalates (POMs) (see Figure 1).[54−56] MNPs have precisely defined chemical structures, sizes, shape symmetry, and surface functional groups. They are a new class of building blocks (or so-called "nano-atoms") in the construction of giant molecules and engineering of nanostructures. Molecular Janus particles are one subclass of these giant molecules.[57,58] Two representative examples of molecular Janus particles have been reported so far.[39,59] Their self-assembly behaviors are dictated by symmetry breaking in both molecular geometry and chemical interactions. Because of the similar sizes and chemical incompatibility of different MNPs, only ordered 3D double-layered structures have been observed in the bulk. It is highly desired to develop a general strategy to prevent the crystal growth along the lamellar normal direction for the fabrication of 2D nanocrystals.

We envision that molecular Janus particles composed of hydrophobic crystalline MNPs and hydrophilic ionic MNPs could provide a new and practical platform for directing the growth of 2D nanocrystals using electrostatic repulsion. Directional crystallization of the crystalline MNPs in polar solvents leads to 2D nanocrystal formation. The stacking of these 2D nanocrystals may be prohibited by the repulsive interactions introduced by the charges on the surface of MNPs. In this contribution, we report a potentially general strategy to create 2D nanocrystals from MNP-based molecular Janus particles.

RESULTS AND DISCUSSION

Molecular Design and 2D Crystal Formation. As a general rule, the crystallization of amphiphiles is governed by the spatial segregation of the amphiphilic moieties. The main factors that affect the crystallization process and the resulting structures can be investigated in detail based on the various combinations of shapes, polarity, etc., provided by the molecules.[60] To extend the family of nonspherical molecular Janus particles constructed by MNPs, four types of MNPs are

dx.doi.org/10.1021/ja504497h | J. Am. Chem. Soc. 2014, 136, 10691−10699

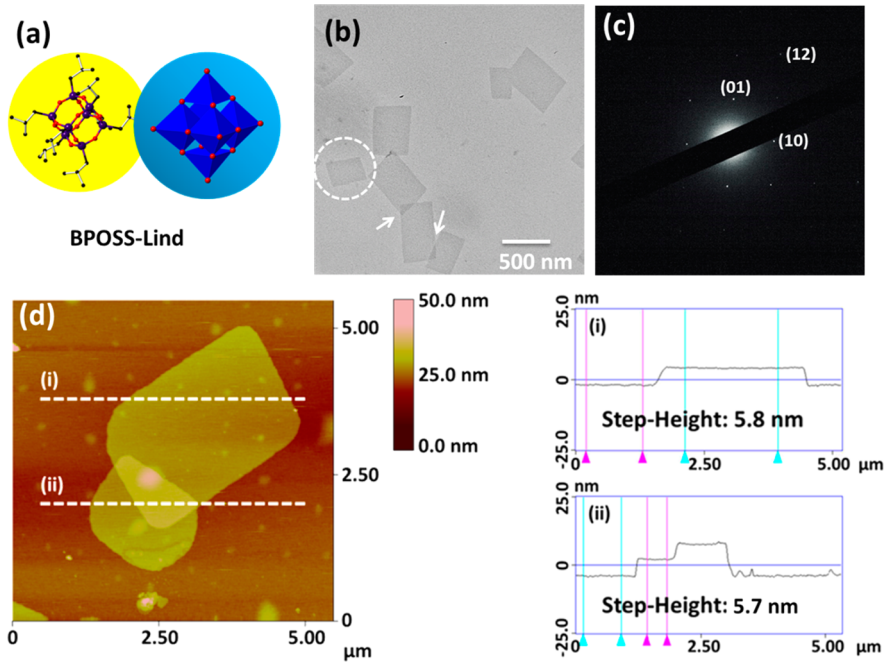

Figure 2. (a) Cartoon illustration of **BPOSS-Lind**. (b) Bright field TEM image of the 2D nanocrystals from slow evaporation of **BPOSS-Lind**/acetonitrile solution. The initial concentration is 0.1 mg/mL. The white arrows indicate the overlapped regions. Scale bar: 500 nm. (c) SAED patterns of one nanocrystal as indicated with the white circle in (b). (d) AFM image in the height mode and the step-height analysis of the 2D nanocrystals.

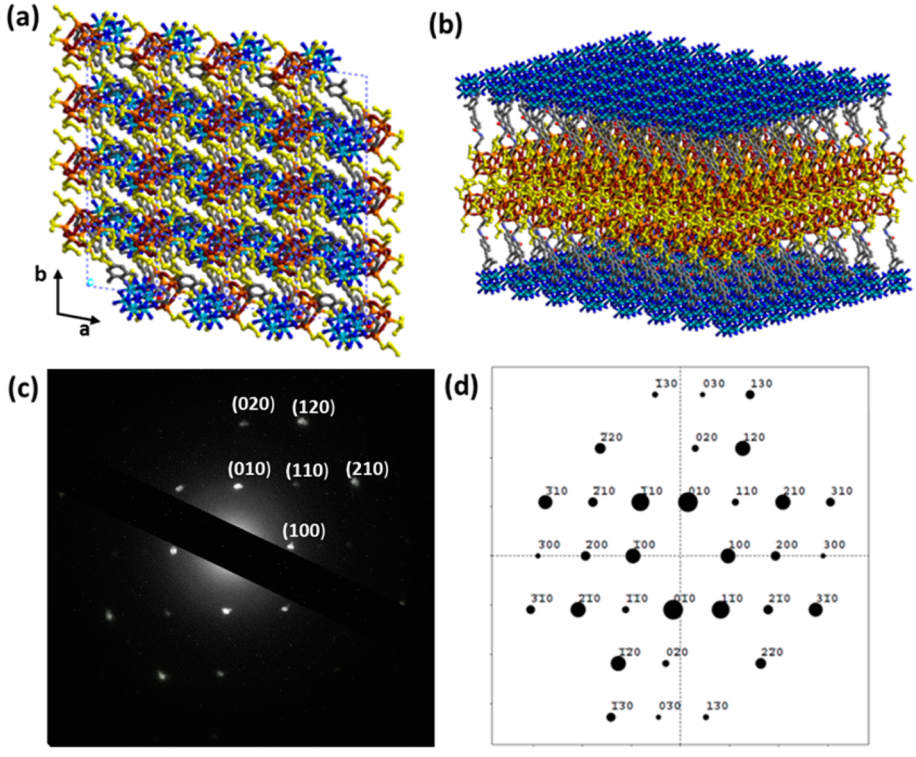

Figure 3. Top view (a) and side-view (b) of the simulated molecular arrangements in the 2D plane lattice of the **BPOSS-Lind** nanocrystals. (c) SAED patterns of the bulk crystal along the [001] zone. (d) Simulated electron diffraction patterns along the [001] zone. The counterions are omitted in (a) and (b) for clarity.

selected as the building blocks in this study, and their chemical structures and estimated sizes are shown in Figure 1a. Three sets of molecular Janus particles, namely, **BPOSS-Lind**, **BPOSS-APOSS**, and **BPOSS-AC$_{60}$/DiBPOSS-AC$_{60}$** (see Figure 1a), were designed and synthesized, which share a common structural feature as the combination of one or two crystalline hydrophobic MNPs and one ionic hydrophilic MNP (see Figure 1b). Their Janus nature is introduced by the distinct functionalities of the compositional MNPs. We indeed obtained 2D nanocrystals of these molecular Janus particles under a

dx.doi.org/10.1021/ja504497h | J. Am. Chem. Soc. 2014, 136, 10691−10699

range of experimental conditions. Further investigation revealed several critical factors in the formation of 2D nanocrystals, including the role of solvent, degree of ionization of MNPs and relative size of paired MNPs, as analyzed by the structure and morphology of the crystals. To the best of our knowledge, this is the first report to generate 2D nanocrystals from self-assembly of MNP-based molecular Janus particles.

Effect of Solvent on the Formation of 2D Nanocrystals. As BPOSS derivatives have strong tendency to crystallize by themselves, they are ideal candidates as the hydrophobic crystalline MNP.[39,61,62] Polyoxometalates (POMs) are metal−oxygen anionic clusters composed of early transition metals (most commonly molybdenum, vanadium and tungsten) in their high oxidation states and other heteroatoms (such as silicon and phosphorus).[63] They provide an extensive family of ionic MNPs with tunable sizes, varied symmetries, selective chemical modification capabilities, and physical properties. A POSS-POM conjugate (**BPOSS-Lind**, see Figure 2a) is synthesized as an amphiphilic molecular Janus particle via the well-established palladium-catalyzed Sonogashira reaction to form a chemical linkage between BPOSS and Lindqvist-POM in good yields.[64−66] Experimental details for synthesis and characterization data of **BPOSS-Lind** are provided in the Supporting Information (SI). The Lindqvist-type POM framework (hexamolybdate $[Mo_6O_{19}]^{2-}$) is selected due to its well-developed functionalization chemistry and its comparable size to the BPOSS cluster (ca. 1.1 nm). The metal−oxygen core size is around 0.8 nm, but taking two delocalized counterions (tetrabutylammonium, TBA) into consideration, the overall size of Lindqvist POM reaches ca. 1.0 nm (Figure 1a).[67] The amphiphilicity of **BPOSS-Lind** stems from the nonpolar BPOSS cage and the highly polar, ionic Lindqvist-type POM moiety.

2D nanosheets can be obtained by evaporation of a dilute **BPOSS-Lind** solution (0.01 wt %) in acetonitrile, which is a good solvent for Lindqvist-POM, but a poor solvent for BPOSS. Figure 2b is a bright-field transmission electron microscopy (TEM) image of the resulting 2D nanosheets and shows regular rhombic shaped nanocrystals with lateral sizes in the micrometer scale. The selected area electron diffraction (SAED) pattern of one individual 2D nanosheet (circled in Figure 2b) displays four diffraction pairs (Figure 2c), indicating an ordered periodic arrangement of the molecular Janus particles along the direction perpendicular to the 2D nanocrystal normal. Atomic force microscopy (AFM) in the height mode (Figure 2d) indicates a thickness of 5.7 ± 0.2 nm. This value is about twice the length of the **BPOSS-Lind** molecular Janus particle along the longest axis (3.0 nm). Strictly speaking, the self-assembled 2D structure is a limited 3D assembly, since two layers of molecular Janus particles stack along the layer normal direction. For simplicity, we called such self-assembled nanosheets as 2D nanocrystals. From the SAED pattern, the packing arrangement of the **BPOSS-Lind** molecular Janus particles within the 2D plane lattice can be described by an oblique *p*-lattice unit cell (Figure 3a).

Similar observations also apply to other polar solvents, such as dimethylformamide (DMF), in which **BPOSS-Lind** forms 2D nanocrystals, too (Figure S1a (SI)). It should also be noted that both temperature and partial pressure of the solvent vapor during evaporation govern the crystal growth kinetics. Slower solvent evaporation at ambient temperature yields 2D nanocrystals with larger lateral sizes and more regular crystal shapes than those grown at elevated temperatures (data not shown). Generally speaking, an environment with lower isothermal temperature and higher solvent vapor pressure could help slow down the crystallization kinetics, leading to quality 2D nanocrystals.

The next question is how to correlate this 2D lattice (Figure 2c) with the 3D crystal structure of this **BPOSS-Lind** molecular Janus particle. We found that when switching the solvent to acetone with lower dielectric constant, different self-assembled morphologies are observed (see Figure S1b (SI)). The SAED pattern displays many sets of strong diffraction spots within one reciprocal lattice (see Figure S1c (SI)), suggesting that these crystals are composed of a crystallographic stacking of multiple layers and thus, are 3D crystals. The small-angle X-ray scattering (SAXS) profile only shows one diffraction peak at 5.48 nm (Figure S2a (SI)), while the wide-angle X-ray diffraction (WAXD) pattern (Figure S2b (SI)) displays many sharp diffraction peaks. Combining SAXS and WAXD data with the SAED results of the 3D crystals, we determined that the **BPOSS-Lind** 3D crystals possess a triclinic unit cell with a = 1.05 nm, b = 0.92 nm, c = 5.48 nm, α = 95.6°, β = 98.1°, and γ = 96.9° (see the SI for details) with a $P\bar{1}$ cell symmetry and two **BPOSS-Lind** molecules per unit cell (Z = 2). The measured density of the crystal is 1.47 g/cm^3, which is in good agreement with the calculated density (1.48 g/cm^3). Molecular modeling and crystal packing analysis with the Accelrys Cerius^2 software yields a possible structure of the **BPOSS-Lind** bulk crystals grown from the acetone solution, from which molecular arrangement in the 2D crystals can be deduced (Figures 3a,b). The inner bilayer is made of the crystalline BPOSS cages and the outer layers are the Lindqvist-POM clusters surrounded by positively charged tetrabutylammonium (TBA) counterions (which are not shown in these two figures for clarity). It is thus evident the observed SAED pattern of the **BPOSS-Lind** 3D crystal along the [001] zone as shown in Figure 3c not only matches well with the simulated ED pattern (Figure 3d), but also share obvious similarity to that shown in Figure 2c, indicating that the 2D nanocrystals do have the same molecular packing as that in the *ab* plane of the 3D **BPOSS-Lind** crystals.

The formation of 2D nanocrystals may also be influenced by the initial concentration of the molecular Janus particles in solution, in addition to the nature of solvent. Multilayered nanocrystals were usually obtained in acetonitrile solutions of **BPOSS-Lind** with higher initial concentrations (0.03 wt %, Figure S3a (SI)). However, the SAED pattern (Figure S3b (SI)) indicates that there is no crystallographic correlation among the layers, revealing that these nanocrystals were independently grown from each other and only stack up during solvent evaporation. It is then concluded that increasing the initial concentration of the molecular Janus particles only affects the nucleation density of 2D nanocrystals (and thus, the number of the crystals). Therefore, initial concentrations of molecular Janus particles and isothermal temperature during solvent evaporation are found to affect mainly the nucleation and crystal growth kinetics, rather than changing the topology and dimensionality of the resulting crystals.

Driven by the enthalpic interactions of the BPOSS cages, directional crystallization first occurs to form the 2D layered structures. For **BPOSS-Lind**, as the 2D nanocrystals are formed in polar solvents, TBA cations form a diffuse layer around the 2D nanocrystals, leaving the surface occupied by Lindqvist-POMs with overall net negative charges. These charged surfaces prevent further aggregation of the layers along the

dx.doi.org/10.1021/ja504497h | J. Am. Chem. Soc. 2014, 136, 10691−10699

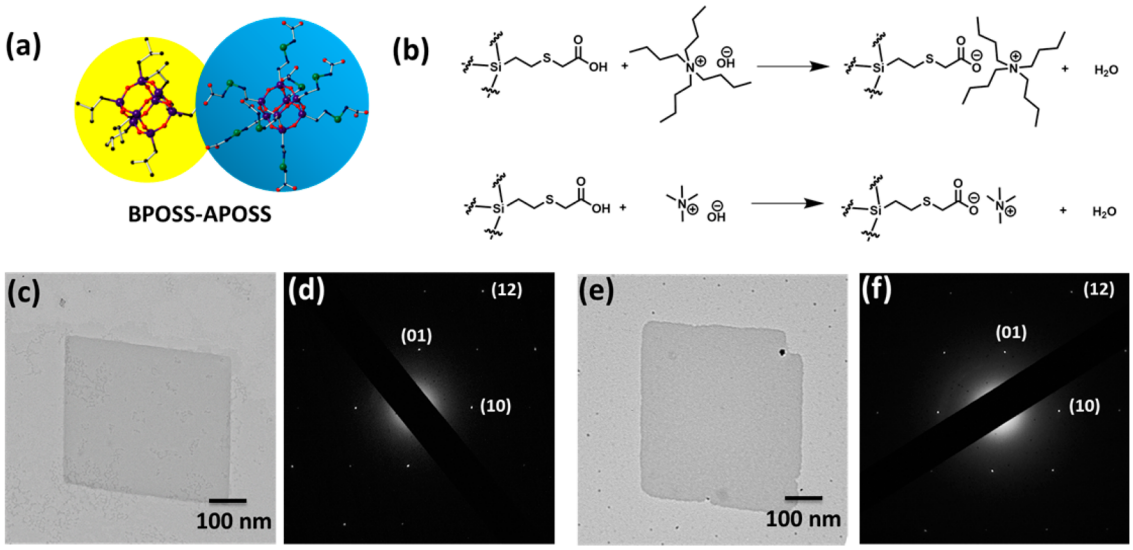

Figure 4. (a) Cartoon illustration of **BPOSS-APOSS**. (b) Neutralization reactions between carboxylic acid groups and tetrabutylammonium hydroxide (TBAOH) or tetramethylammonium hydroxide (TMAOH). (c) Bright field TEM image of 2D nanocrystals from slow evaporation of **BPOSS-APOSS**/methanol/DMF solution mixed with TBAOH in a 1:2 molar ratio. (d) Selected area electron diffraction (SAED) patterns of one 2D nanocrystal in (c). (e) Bright field TEM image of 2D nanocrystals from slow evaporation of **BPOSS-APOSS**/methanol/DMF solution mixed with TMAOH in a 1:2 molar ratio. (f) SAED patterns of the nanocrystal shown in (e).

layer normal direction and thus, stabilize the 2D structure. In less polar solvents such as acetone, the repulsive forces are largely reduced due to poor solvating of the TBA ions, and 3D crystals are thus resulted. In order to provide more evidence for this speculation, we need to illustrate how the formation of 2D nanocrystals is affected by the ionic MNPs and the property of the positive counterions. However, in the case of **BPOSS-Lind**, Lindqvist POM is a bivalent cluster and each POM must be bounded with two counterions. To freely tune the number and species of the counterions, we need to use different molecular Janus particles.

Effect of Number and Size of Counterions. The effect of counterions is best illustrated in **BPOSS-APOSS** (see Figure 4a), which is composed of a hydrophobic isobutyl-substituted BPOSS and a hydrophilic APOSS substituted with seven carboxylic acid groups, similar to the previously described molecular Janus particle.[39] Synthesis of **BPOSS-APOSS** is straightforward and the experimental details and characterization data are summarized in the SI. Most importantly, carboxylic acid groups on the APOSS MNP can be neutralized with tetrabutylammonium hydroxide (TBAOH) (see Figure 4b), resulting in ionized APOSS cages with a tunable number of charges.

BPOSS-APOSS with no counterions crystallizes in a polar mixed solvent of methanol/DMF (v/v = 95/5). Slow evaporation of a solution with initial concentration ranging from 0.05 to 0.5 mg/mL yields only multiple-stacked crystal layers (Figure S5 (SI)). Their SAED patterns display pairs of BPOSS diffraction spots generated within a single reciprocal lattice, indicating the formation of 3D **BPOSS-APOSS** crystals, as previously reported.[39] To validate the hypothesis that charged MNPs are essential for the formation of 2D (as opposed to 3D) nanocrystals, the same counterions (namely, TBA) are introduced. The molar ratios of **BPOSS-APOSS** and TBAOH in the neutralization are varied. The corresponding products are denoted as **BPOSS-APOSS-nTBA**, where **n** is the average number of TBA ions per APOSS. The neutralization state can be monitored by Fourier transform infrared (FT-IR) via the relative strength of the absorption bands of the -COOH and $-COO^-$ groups (Figure S6 (SI)). It should be noted that the neutralization reaction is only analyzed by defining a specific average number of TBA ions for each APOSS cage.

Solvent evaporation of the **BPOSS-APOSS-2TBA** solution in MeOH/DMF yields the 2D nanocrystals shown in Figure 4c. The SAED pattern (Figure 4d) is strikingly similar to that of the **BPOSS-Lind** 2D nanocrystals shown in Figure 2b. AFM measurements give rise to a crystal thickness of 4.5 ± 0.2 nm, close to twice the **BPOSS-APOSS** length along the molecular long axis (Figure S7a (SI)). With four counterions per APOSS, the crystal size is significantly reduced to sub-100 nm as shown in Figure S8b (SI). When the number of counterions per molecule is further increased, only fragmented or dendritic aggregations are observed (Figure S8c (SI)). This set of experiments with a varying number of TBA ions per molecule clearly confirms the significant role of negatively charged MNPs in the growth process of 2D nanocrystals. In the absence of any counterions, the strong hydrogen bonding between carboxyl groups on APOSS cages within and between layers allows crystal growth along the layer normal direction and thus, results in 3D crystals. With two counterions per APOSS cage, the electrostatic repulsive interaction prevents aggregation of the 2D double layers along the normal direction and therefore, results in facetted 2D nanocrystals. When having even more counterions, the lateral growth of the BPOSS cage crystals is also hampered. The resulting fragmented or dendritic crystal morphologies suggest that the stronger electrostatic interactions between the APOSS-6TBA segments and the expanded conformations of the POSS heads tend to cover the lateral edges of the center BPOSS core, and thus, limiting the lateral crystal size.

The impact of the counterion size on the formation of 2D nanocrystals has also been investigated by using tetramethylammonium hydroxide (TMAOH) with a smaller cation, instead of TBAOH. The results show very little, if any, difference between these two counterions, as illustrated in Figure 4e. The crystal morphology, SAED (Figure 4f), and even

dx.doi.org/10.1021/ja504497h | J. Am. Chem. Soc. 2014, 136, 10691−10699

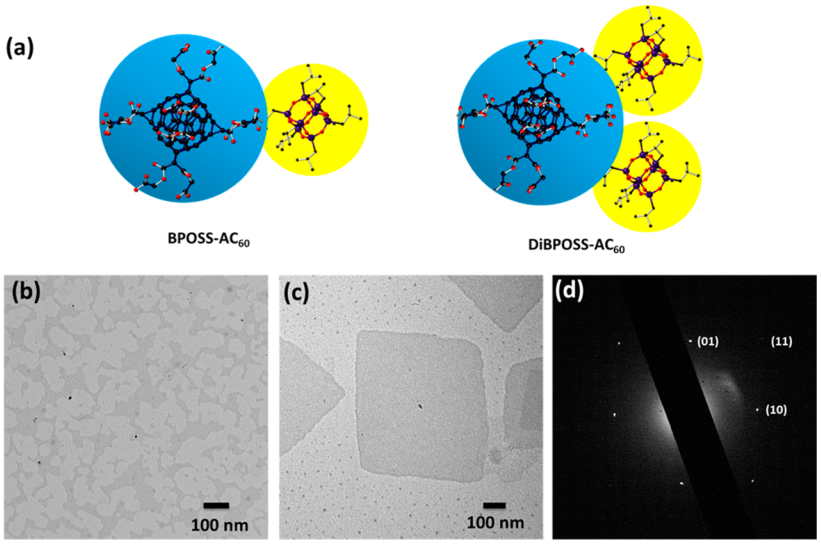

Figure 5. (a) Cartoon illustrations of **BPOSS-AC$_{60}$** and **DiBPOSS-AC$_{60}$**. (b) Bright field TEM image by slow evaporation from **BPOSS-AC$_{60}$**/TBAOH (1/4 molar ratio) methanol solution. (c) Bright field TEM image of 2D nanocrystals from slow evaporation of **DiBPOSS-AC$_{60}$**/TBAOH (1/4 molar ratio) methanol solution. (d) SAED patterns of the nanocrystal shown in (c).

Table 1. Summary of Conditions for Well-Defined 2D Nanocrystals

sample	solvent	counter ion	molar ratio[b]	density (g/cm^3)	thickness[c] (nm)	specific surface area[d] (m^2/g)
BPOSS-Lind	CH_3CN	TBA	1:2	1.47	5.7 ± 0.2	238
BPOSS-APOSS	MeOH/DMF[a]	TBA/TMA	1:2	1.50	4.5 ± 0.2	296
BPOSS-AC$_{60}$	N/A	N/A	N/A	N/A	N/A	N/A
DiBPOSS-AC$_{60}$	MeOH/DMF[a]	TBA	1:4	1.35	5.2 ± 0.2	283

[a]The volume ratio of MeOH to DMF is 95/5. [b]The molar ratio refers to molecular Janus particle to counterions. [c]The thickness is a statistical value of more than 15 samples measured by AFM. [d]Calculation of specific surface area is illustrated in the SI.

crystal thickness (4.4 ± 0.2 nm, an AFM result in Figure S7b (SI)) are similar. With increasing the counterion ratio, the crystal size decreases for **BPOSS-APOSS-4TMA** and no regular 2D nanocrystals could be formed in **BPOSS-APOSS-6TMA** solution. In this case, the number of counterions per molecule also likely plays a major role in the crystal growth of 2D nanocrystals.

Effect of MNP Size Matching on 2D Crystal Formation. As an analysis, a one-to-one conjugate of MNPs with unbalanced sizes should not favor a flat morphology.[68] In the above-mentioned amphiphiles, the sizes of the hydrophobic and ionic MNPs are close to each other, and lamellar structures are thus expected. In order to reveal the effect of MNP size matching, we designed and synthesized two related molecular Janus particles, **BPOSS-AC$_{60}$** and **DiBPOSS-AC$_{60}$**. In these materials, the diameter of the carboxyl-functionalized AC$_{60}$ (∼ 1.5 nm) is significantly larger than that of the BPOSS (∼ 1.1 nm) (Figure 1). The synthesis is fully described and discussed in the SI. Each AC$_{60}$ has 10 carboxylic acid groups, which can be similarly ionized by adding TBAOH.

No regular facetted 2D nanocrystals were observed when TBAOH was added to the solution of **BPOSS-AC$_{60}$** in methanol/DMF (v/v = 95/5) to tune the number of counterions per AC$_{60}$ from 2 to 10 (Figure 5b). In contrast, facetted 2D nanocrystals were obtained in **DiBPOSS-A$_{60}$-nTBA** solutions, especially at an optimized **n** value of 4, as shown in Figure 5c and Figure S9 (SI). The SAED pattern (Figure 5d) is almost identical to those of the above 2D nanocrystals, indicating that the crystal structure is again dominated by the BPOSS cages. These observations validate our speculation that size matching is a major determining factor in the formation of 2D nanocrystals. The significant size mismatch between the two MNPs in **BPOSS-AC$_{60}$** hinders or even prohibits crystallization of the BPOSS cages. Only when the overall interfacial area of the crystalline BPOSS is equal to or slightly larger than that of AC$_{60}$ (as in the case of **DiBPOSS-AC$_{60}$**) can the 2D nanocrystals be formed. Comparing crystallization behaviors of these two samples also suggests that only the double-layered arrangement of BPOSS moiety is stable enough to form the 2D nanocrystals, since **BPOSS-AC$_{60}$** failed to generate an interdigitated single BPOSS layered structure that would also have provided more surface area to accommodate the size mismatch. The double-layered **DiBPOSS-AC$_{60}$-4TBA** 2D nanocrystals are 5.2 ± 0.2 nm thick (Figure S7c (SI)), which matches double the length of the triad molecular Janus particle along the molecular long axis. Because of the size difference of APOSS and AC$_{60}$, the measured thickness of 2D nanocrystals of **DiBPOSS-AC$_{60}$** is slightly greater than that of **BPOSS-APOSS-2TBA** and **BPOSS-APOSS-2TMA**.

Specific surface area is an important parameter of 2D nanocrystals and can be calculated based on the thickness and density of the 2D nanocrystals (see the SI for detailed calculations). For the **BPOSS-Lind** 2D nanocrystals, the specific surface area is 238 m^2/g, while the specific surface areas of the **BPOSS-APOSS-2TBA** and the **DiBPOSS-AC$_{60}$-4TBA** 2D nanocrystals are 296 and 283 m^2/g, respectively. Experimental conditions to generate 2D nanocrystals and their specific surface area values are summarized in Table 1.

dx.doi.org/10.1021/ja504497h | J. Am. Chem. Soc. 2014, 136, 10691−10699

The stability of these 2D nanocrystals is originated from the enthalpic interaction among the crystalline BPOSS cages. Thermal stabilities of the 2D nanocrystals in the solid state can be directly associated with their melting temperatures. As a reference, the 3D crystals of BPOSS-based molecular Janus particles typically have melting points ranging from 150 to 180 °C (Figure S10 (SI)).[39] Therefore, the melting temperatures of these 2D nanocrystals could be estimated based on the Gibbs−Thomson relation[69,70] to be between 70 and 100 °C, assuming that the surface free energy is around 30 erg/cm^2 and the heat of fusion of BPOSS is about 5.8 × 10^8 erg/cm^3.[70,71] Moreover, these crystals do not dissolve in highly polar, protic solvents (such as water) or completely nonpolar solvents (such as hexane). Further assemblies of the 2D nanocrystals with other nonionic building blocks could become possible in those solvents. Nevertheless, the most effective way to further stabilize these 2D nanocrystals is to adopt chemically cross-linkable MNP building blocks into the molecular Janus particle so that the morphology of 2D nanocrystals can be fixed by photochemical cross-linking reactions.[72−75] It should be noted that 2D and even 3D nanostructures with other morphologies are also possible through careful molecular designs and new self-assembly strategies. For example, we have shown recently that 3D hexagonal nanoprisms can be prepared in solution from a specifically designed giant surfactants of a hydrophilic C_{60} tethered with two hydrophobic polystyrene tails.[57]

While our current focus is on understanding the molecular mechanism for the formation of 2D nanocrystals through directional crystallization of molecular Janus particles, we expect that these 2D nanocrystals may possess similar structural features common to other low-dimensional materials.[11−28] Specifically, POM may be used as a building block of Janus particles in these 2D nanocrystals to control the surface properties, to make structurally reinforced composites, as well as in applications such as catalysis,[76] electrochemistry,[77] photochromism,[78] magnetism[79] to medicine.[80] We are currently investigating some of those applications using our 2D nanocrystals.

CONCLUSION

Self-assembled 2D nanocrystals made of MNP-based molecular Janus particles are obtained without the assistance of templates or in a confined environment. A series of **BPOSS-LIND**, **BPOSS-APOSS**, **BPOSS-AC$_{60}$**, and **DiBPOSS-AC$_{60}$**, have been synthesized for a systematic study of their structures and formation conditions (solvent, number and size of counterions and size of MNPs, see Table 1). They are all composed of hydrophobic crystalline MNPs (BPOSS cages in this case) and ionic MNPs. Under selected conditions, unique self-assembled 2D nanocrystals made of double layers are obtained. The double layers of crystalline BPOSS cages are sandwiched between two layers of ionic MNPs. In selected polar solvents (acetonitrile, DMF, or methanol), solvation of the counterions creates partially charged 2D nanocrystals and thus, generates repulsive electrostatic interactions that limit or suppress aggregation along the layer normal direction. The role of counterions has been analyzed by tuning both the number and size of counterions that are bounded to the APOSS in BPOSS-APOSS molecular Janus particle. Without counterions, stacks of 2D layers can be obtained due to the interlayer hydrogen bonding between the APOSS, leading to the formation of a 3D crystal. When partially neutralized with TBAOH, the competitive electrostatic repulsive interactions overcome the interlayer hydrogen bonds between the APOSS, resulting in 2D nanocrystals. However, adding too many charges associated with one APOSS will eventually also prevent the lateral growth of the molecular Janus particle crystals. The issue of size matching becomes a very stringent requirement in the present system since the structure has to remain flat. Because of the rigid conformation and persistent shape, molecular Janus particles with unbalanced MNP component sizes could not yield e.g. cylinder or sphere structures with a large curved interface. Thus, when the size is too unbalanced, the material does not crystallize (e.g., **BPOSS-AC$_{60}$**). It is only when two BPOSS cages are attached to AC_{60} that a 2D layer can be formed. The structural organization of the building blocks in the crystal is further illustrated by the fact that in all those materials, bilayers are formed. The dimension matching is not achieved by formation of a single layer with interdigitated BPOSS cages that would double the interface area. This study has general implications on understanding of 2D nanocrystal formation and opens a bottom-up approach toward fabrication of well-defined 2D nanostructures with potential technologically relevant applications.

ASSOCIATED CONTENT

Supporting Information

The experimental details, additional results and discussion are provided. This material is available free of charge via the Internet at http://pubs.acs.org.

AUTHOR INFORMATION

Corresponding Authors

wenbin@pku.edu.cn
ky13@zips.uakron.edu
scheng@uakron.edu

Notes

The authors declare no competing financial interest.

ACKNOWLEDGMENTS

This work is supported by NSF (DMR-1408872) and the Joint-Hope Foundation.

REFERENCES

(1) Lehn, J. *Science* **1993**, *260*, 1762−1763.
(2) Hawker, C. J.; Wooley, K. L. *Science* **2005**, *309*, 1200−1205.
(3) Whitesides, G. M.; Boncheva, M. *Proc. Natl. Acad. Sci. U. S. A.* **2002**, *99*, 4769−4774.
(4) Hartgerink, J. D.; Beniash, E.; Stupp, S. I. *Science* **2001**, *294*, 1684−1688.
(5) Hill, J. P.; Jin, W.; Kosaka, A.; Fukushima, T.; Ichihara, H.; Shimomura, T.; Ito, K.; Hashizume, T.; Ishii, N.; Aida, T. *Science* **2004**, *304*, 1481−1483.
(6) Zhang, L.; Eisenberg, A. *Science* **1995**, *268*, 1728−1731.
(7) Kuzyk, A.; Schreiber, R.; Fan, Z. Y.; Pardatscher, G.; Roller, E. M.; Hogele, A.; Simmel, F. C.; Govorov, A. O.; Liedl, T. *Nature* **2012**, *483*, 311−314.
(8) Wang, Z. Y.; Zhou, L.; Lou, X. W. *Adv. Mater.* **2012**, *24*, 1903−1911.
(9) Chen, J. N.; Badioli, M.; Alonso-Gonzalez, P.; Thongrattanasiri, S.; Huth, F.; Osmond, J.; Spasenovic, M.; Centeno, A.; Pesquera, A.; Godignon, P.; Elorza, A. Z.; Camara, N.; de Abajo, F. J. G.; Hillenbrand, R.; Koppens, F. H. L. *Nature* **2012**, *487*, 77−81.
(10) Moughton, A. O.; Hillmyer, M. A.; Lodge, T. P. *Macromolecules* **2012**, *45*, 2−19.

(11) Novoselov, K. S.; Geim, A. K.; Morozov, S. V.; Jiang, D.; Zhang, Y.; Dubonos, S. V.; Grigorieva, I. V.; Firsov, A. A. *Science* **2004**, *306*, 666−669.
(12) Coleman, J. N.; Lotya, M.; O'Neill, A.; Bergin, S. D.; King, P. J.; Khan, U.; Young, K.; Gaucher, A.; De, S.; Smith, R. J.; Shvets, I. V.; Arora, S. K.; Stanton, G.; Kim, H.-Y.; Lee, K.; Kim, G. T.; Duesberg, G. S.; Hallam, T.; Boland, J. J.; Wang, J. J.; Donegan, J. F.; Grunlan, J. C.; Moriarty, G.; Shmeliov, A.; Nicholls, R. J.; Perkins, J. M.; Grieveson, E. M.; Theuwissen, K.; McComb, D. W.; Nellist, P. D.; Nicolosi, V. *Science* **2011**, *331*, 568−571.
(13) Lee, K. Y.; Lim, J. R.; Rho, H.; Choi, Y. J.; Choi, K. J.; Park, J. G. *Appl. Phys. Lett.* **2007**, *91*, 201901.
(14) Sasaki, T.; Watanabe, M. *J. Phys. Chem. B* **1997**, *101*, 10159−10161.
(15) Allen, M. R.; Thibert, A.; Sabio, E. M.; Browning, N. D.; Larsen, D. S.; Osterloh, F. E. *Chem. Mater.* **2010**, *22*, 1220−1228.
(16) Fukuda, K.; Akatsuka, K.; Ebina, Y.; Ma, R.; Takada, K.; Nakai, I.; Sasaki, T. *ACS Nano* **2008**, *2*, 1689−1695.
(17) Osada, M.; Akatsuka, K.; Ebina, Y.; Funakubo, H.; Ono, K.; Takada, K.; Sasaki, T. *ACS Nano* **2010**, *4*, 5225−5232.
(18) Osada, M.; Sasaki, T. *J. Mater. Chem.* **2009**, *19*, 2503−2511.
(19) Sakai, N.; Ebina, Y.; Takada, K.; Sasaki, T. *J. Am. Chem. Soc.* **2004**, *126*, 5851−5858.
(20) Ma, R.; Sasaki, T. *Adv. Mater.* **2010**, *22*, 5082−5104.
(21) Son, J. S.; Yu, J. H.; Kwon, S. G.; Lee, J.; Joo, J.; Hyeon, T. *Adv. Mater.* **2011**, *23*, 3214−3219.
(22) Li, L.; Chen, Z.; Hu, Y.; Wang, X.; Zhang, T.; Chen, W.; Wang, Q. *J. Am. Chem. Soc.* **2013**, *135*, 1213−1216.
(23) Liu, Z.; Ma, R.; Osada, M.; Iyi, N.; Ebina, Y.; Takada, K.; Sasaki, T. *J. Am. Chem. Soc.* **2006**, *128*, 4872−4880.
(24) Li, B.; Li, C. Y. *J. Am. Chem. Soc.* **2006**, *129*, 12−13.
(25) Podsiadlo, P.; Kaushik, A. K.; Arruda, E. M.; Waas, A. M.; Shim, B. S.; Xu, J. D.; Nandivada, H.; Pumplin, B. G.; Lahann, J.; Ramamoorthy, A.; Kotov, N. A. *Science* **2007**, *318*, 80−83.
(26) Allen, M. J.; Tung, V. C.; Kaner, R. B. *Chem. Rev.* **2009**, *110*, 132−145.
(27) Li, X.; Cai, W.; An, J.; Kim, S.; Nah, J.; Yang, D.; Piner, R.; Velamakanni, A.; Jung, I.; Tutuc, E.; Banerjee, S. K.; Colombo, L.; Ruoff, R. S. *Science* **2009**, *324*, 1312−1314.
(28) Seo, J.-w.; Jun, Y.-w.; Park, S.-w.; Nah, H.; Moon, T.; Park, B.; Kim, J.-G.; Kim, Y. J.; Cheon, J. *Angew. Chem., Int. Ed.* **2007**, *46*, 8828−8831.
(29) Vaughn, D. D.; In, S.-I.; Schaak, R. E. *ACS Nano* **2011**, *5*, 8852−8860.
(30) Ithurria, S.; Bousquet, G.; Dubertret, B. *J. Am. Chem. Soc.* **2011**, *133*, 3070−3077.
(31) Tang, Z.; Zhang, Z.; Wang, Y.; Glotzer, S. C.; Kotov, N. A. *Science* **2006**, *314*, 274−278.
(32) Schliehe, C.; Juarez, B. H.; Pelletier, M.; Jander, S.; Greshnykh, D.; Nagel, M.; Meyer, A.; Foerster, S.; Kornowski, A.; Klinke, C.; Weller, H. *Science* **2010**, *329*, 550−553.
(33) Yu, T.; Lim, B.; Xia, Y. *Angew. Chem., Int. Ed.* **2010**, *49*, 4484−4487.
(34) Kato, T.; Mizoshita, N.; Kishimoto, K. *Angew. Chem., Int. Ed.* **2006**, *45*, 38−68.
(35) Nam, K. T.; Shelby, S. A.; Choi, P. H.; Marciel, A. B.; Chen, R.; Tan, L.; Chu, T. K.; Mesch, R. A.; Lee, B. C.; Connolly, M. D.; Kisielowski, C.; Zuckermann, R. N. *Nat. Mater.* **2010**, *9*, 454−460.
(36) Yu, B.; Jiang, X.; Yin, J. *Macromolecules* **2012**, *45*, 7135−7142.
(37) Yu, B.; Jiang, X.; Yin, J. *Chem. Commun.* **2013**, *49*, 603−605.
(38) de Gennes, P.-G. *Angew. Chem., Int. Ed.* **1992**, *31*, 842−845.
(39) Li, Y.; Zhang, W.-B.; Hsieh, I. F.; Zhang, G.; Cao, Y.; Li, X.; Wesdemiotis, C.; Lotz, B.; Xiong, H.; Cheng, S. Z. D. *J. Am. Chem. Soc.* **2011**, *133*, 10712−10715.
(40) Yan, J.; Bloom, M.; Bae, S. C.; Luijten, E.; Granick, S. *Nature* **2012**, *491*, 578−581.
(41) Chen, Q.; Whitmer, J. K.; Jiang, S.; Bae, S. C.; Luijten, E.; Granick, S. *Science* **2011**, *331*, 199−202.
(42) Dendukuri, D.; Pregibon, D. C.; Collins, J.; Hatton, T. A.; Doyle, P. S. *Nat. Mater.* **2006**, *5*, 365−369.
(43) Nie, Z.; Li, W.; Seo, M.; Xu, S.; Kumacheva, E. *J. Am. Chem. Soc.* **2006**, *128*, 9408−9412.
(44) Nisisako, T.; Torii, T.; Takahashi, T.; Takizawa, Y. *Adv. Mater.* **2006**, *18*, 1152−1156.
(45) Shepherd, R. F.; Conrad, J. C.; Rhodes, S. K.; Link, D. R.; Marquez, M.; Weitz, D. A.; Lewis, J. A. *Langmuir* **2006**, *22*, 8618−8622.
(46) Walther, A.; Andre, X.; Drechsler, M.; Abetz, V.; Mueller, A. H. E. *J. Am. Chem. Soc.* **2007**, *129*, 6187−6198.
(47) Liu, Y. F.; Abetz, V.; Muller, A. H. E. *Macromolecules* **2003**, *36*, 7894−7898.
(48) Yang, J.; Elim, H. I.; Zhang, Q.; Lee, J. Y.; Ji, W. *J. Am. Chem. Soc.* **2006**, *128*, 11921−11926.
(49) Gu, H. W.; Zheng, R. K.; Zhang, X. X.; Xu, B. *J. Am. Chem. Soc.* **2004**, *126*, 5664−5665.
(50) Laine, R. M. *J. Mater. Chem.* **2005**, *15*, 3725−3744.
(51) Roll, M. F.; Asuncion, M. Z.; Kampf, J.; Laine, R. M. *ACS Nano* **2008**, *2*, 320−326.
(52) Zhang, W.-B.; Tu, Y.; Ranjan, R.; Van Horn, R. M.; Leng, S.; Wang, J.; Polce, M. J.; Wesdemiotis, C.; Quirk, R. P.; Newkome, G. R.; Cheng, S. Z. D. *Macromolecules* **2008**, *41*, 515−517.
(53) Yu, X.; Zhang, W.-B.; Yue, K.; Li, X.; Liu, H.; Xin, Y.; Wang, C.-L.; Wesdemiotis, C.; Cheng, S. Z. D. *J. Am. Chem. Soc.* **2012**, *134*, 7780−7787.
(54) Coronado, E.; Gómez-García, C. J. *Chem. Rev.* **1998**, *98*, 273−296.
(55) Katsoulis, D. E. *Chem. Rev.* **1998**, *98*, 359−388.
(56) Dolbecq, A.; Dumas, E.; Mayer, C. d. R.; Mialane, P. *Chem. Rev.* **2010**, *110*, 6009−6048.
(57) Yu, X.; Yue, K.; Hsieh, I.-F.; Li, Y.; Dong, X.-H.; Liu, C.; Xin, Y.; Wang, H.-F.; Shi, A.-C.; Newkome, G. R.; Ho, R.-M.; Chen, E.-Q.; Zhang, W.-B.; Cheng, S. Z. D. *Proc. Natl. Acad. Sci. U. S. A.* **2013**, *110*, 10078−10083.
(58) Zhang, W.-B.; Yu, X.; Wang, C.-L.; Sun, H.-J.; Hsieh, I.-F.; Li, Y.; Dong, X.-H.; Yue, K.; Van Horn, R. M.; Cheng, S. Z. D. *Macromolecules* **2014**, *47*, 1221−1239.
(59) Sun, H.-J.; Tu, Y.; Wang, C.-L.; Van Horn, R. M.; Tsai, C.-C.; Graham, M. J.; Sun, B.; Lotz, B.; Zhang, W.-B.; Cheng, S. Z. D. *J. Mater. Chem.* **2011**, *21*, 14240−14247.
(60) Moulton, B.; Zaworotko, M. J. *Chem. Rev.* **2001**, *101*, 1629−1658.
(61) Larsson, K. *Ark. Kemi* **1960**, *16*, 203−208.
(62) Larsson, K. *Ark. Kemi* **1960**, *16*, 209−214.
(63) Proust, A.; Matt, B.; Villanneau, R.; Guillemot, G.; Gouzerh, P.; Izzet, G. *Chem. Soc. Rev.* **2012**, *41*, 7605−7622.
(64) Wei, Y.; Xu, B.; Barnes, C. L.; Peng, Z. *J. Am. Chem. Soc.* **2001**, *123*, 4083−4084.
(65) Chinchilla, R.; Nájera, C. *Chem. Rev.* **2007**, *107*, 874−922.
(66) Wu, P.; Li, Q.; Ge, N.; Wei, Y.; Wang, Y.; Wang, P.; Guo, H. *Eur. J. Inorg. Chem.* **2004**, *2004*, 2819−2822.
(67) Pope, M. T.; Müller, A. *Angew. Chem., Int. Ed.* **1991**, *30*, 34−48.
(68) Lotz, B.; Cheng, S. Z. D. *Polymer* **2005**, *46*, 577−610.
(69) Cheng, S. Z. D. *Nature* **2007**, *448*, 1006−1007.
(70) Dong, X.-H.; Van Horn, R.; Wurm, A.; Schick, C.; Lotz, B.; Zhang, W.-B.; Cheng, S. Z. D. *J. Phys. Chem. Lett.* **2013**, *4*, 2356−2360.
(71) Roy, S.; Feng, J.; Scionti, V.; Jana, S. C.; Wesdemiotis, C. *Polymer* **2012**, *53*, 1711−1724.
(72) O'Reilly, R. K.; Hawker, C. J.; Wooley, K. L. *Chem. Soc. Rev.* **2006**, *35*, 1068−1083.
(73) O'Reilly, R. K.; Joralemon, M. J.; Hawker, C. J.; Wooley, K. L. *J. Polym. Sci., Part A: Polym. Chem.* **2006**, *44*, 5203−5217.
(74) Wang, J.; Shen, Y.; Kessel, S.; Fernandes, P.; Yoshida, K.; Yagai, S.; Kurth, D. G.; Möhwald, H.; Nakanshi, T. *Angew. Chem., Int. Ed.* **2009**, *48*, 2166−2170.
(75) Sengupta, S.; Würthner, F. *Chem. Commun.* **2012**, *48*, 5730−5732.

(76) Mizuno, N.; Yamaguchi, K.; Kamata, K. *Coord. Chem. Rev.* **2005**, *249*, 1944−1956.
(77) Katsoulis, D. E. *Chem. Rev.* **1998**, *98*, 359−388.
(78) He, T.; Yao, J. *Prog. Mater. Sci.* **2006**, *51*, 810−879.
(79) Clemente-Juan, J. M.; Coronado, E. *Coord. Chem. Rev.* **1999**, *193*−*195*, 361−394.
(80) Rhule, J. T.; Hill, C. L.; Judd, D. A. *Chem. Rev.* **1998**, *98*, 327−358.